Assessment of Complex Peptide Degradation Pathways via Structured Multicompartmental Modeling Approaches: The Metabolism of Dynorphin A1–13 and Related Fragments in Human Plasma

STEFAN MÜLLER,[†,‡] ALAN HUTSON,[§] V. ARYA,[†] AND GÜNTHER HOCHHAUS*[,†]

Contribution from *Department of Pharmaceutics, College of Pharmacy, University of Florida, Gainesville, Florida 32610.*

Received January 26, 1998. Final revised manuscript received May 10, 1999.
Accepted for publication June 21, 1999.

Abstract □ Peptide metabolic pathways in blood or other tissues are often complex because multiple enzyme systems are involved in the degradation of parent drug and its metabolites. Michaelis–Menten-type studies with isolated enzymes have been frequently employed for evaluating the metabolism of peptides. Alternatively, studies with selective enzyme inhibitors or the evaluation of the area under the drug– or metabolite–time profiles have been employed. We tested in this study the usefulness of a multicompartmental pharmacokinetic approach for the assessment of the apparent first-order metabolism of dynorphin A1–13 up to the fourth metabolite generation in human plasma. This multicompartmental kinetic analysis proved instrumental in clarifying ambiguous degradation pathways not easily detectable by the other methods of assessment (enzyme inhibition studies and noncompartmental analysis) because of the lack of specific enzyme inhibitors or specificity problems of the analytical technique employed. The proposed multicompartmental fitting approach was also highly suitable to verify the overall metabolic pathways suggested by the other methods up to the fourth metabolite by testing whether the rate constants obtained by these methods are suitable to describe the overall degradation profile after Dyn A1–13 degradation. Local sensitivity analysis for the degradation of DYNA 1–13 revealed that the model was, however, not able to adequately identify on its own all of the parameters involved in the degradation of dynorphin A1–13. Thus, the method proved beneficial in evaluating and testing the correctness of the overall degradation pathways suggested by other methods.

Introduction

Biologically active peptides often exert their effects via active metabolites. With the use of peptides as therapeutic agents, a detailed understanding of their metabolism is therefore important. The model peptide Dyn A1−13 used in this study is extensively metabolized in plasma.[1] N-terminally intact metabolic fragments of Dyn A1−13 (Dyn A1−12 through Dyn A1−5) retain opioid receptor affinity,[2] while N-terminally truncated dynorphin derivatives such as Dyn A2−13 modulate morphine tolerance via nonopioid pathways, possibly the NMDA-receptor[3,4] and/or melanocortin receptor.[5]

The in-vitro metabolic pathway of Dyn A1−13 in human plasma is complex, as previously assessed up to the fourth metabolic generation by enzyme inhibition studies and a noncompartmental analysis of the metabolic pathway.[1] Enzyme inhibition studies can only assess the contribution of one enzymatic system to the overall metabolic fate of the parent drug or identified metabolites; and they depend on the specificity of the enzyme inhibitors involved. A noncompartmental (AUC-based) approach introduced in these studies[1] compared the area under the concentration−time profiles of a given metabolite during degradation of the parent drug (e.g., Dyn A1−13) with the area observed after direct degradation of the synthesized metabolite. This approach allows simultaneously monitoring of several metabolites and does not depend on the availability of selective enzyme inhibitors but on the high selectivity of the chromatographic system for the determination of parent drug and metabolites. Because of the limitations found for both methods, this study focuses on the applicability of a structured multicompartmental kinetic analysis (nonlinear curve fitting procedures for apparent first-order kinetic processes) for the analysis of complex metabolic events. The results presented here suggest that this mode of analysis has certain advantages over the above methods and that it should be applied in conjunction with the other methods to assess complex metabolic degradation pathways of peptide drugs.

Materials and Methods

Data—Concentration−time profiles of parent compound (generally Dyn A1−13 or shorter fragments such Dyn A1−12 or Dyn A2−12, Dyn A 3−12, Dyn A 4−12, Dyn A 1−10, Dyn A 2−13) and resulting metabolites obtained after incubation of peptides at 37 °C in neat plasma in the presence or absence of specific enzyme inhibitors (GEMSA, bestatin, captopril, leucinetiol) have been previously described.[1] These data were reanalyzed in this study.

Data Analysis—Differential equations describing sequential and parallel pathways of dynorphin metabolism (see Figures 1 and 2, for the metabolic pathways of Dyn A1−13 investigated, see Figure 1 for final pathway) were established.[6] These equations incorporated the overall rate of degradation of a given peptide (degradation rate constant of DynA1−13: k_1; degradation rate of metabolites: $k_2 - k_7$) and the rate of generation of metabolites (k_{12}, k_{16}, k_{23}, k_{63}, k_{27}...). See Figure 1 for explanation of the abbreviations of rate constants used. The Laplace transform of the concentration of a given dynorphin fragment (as,c) was calculated as the product of the input (ins; here the initial amount of peptide spiked into the incubation solution) and the following modified disposition function ($d_{s,c}$).[7]

$$d_{s,c} = \frac{\prod_{i=2}^{N}(s + k_i)}{\prod_{i=1}^{N}(s + k_i) - \sum_{j=2}^{N}[k_{1j}\prod_{\substack{m=2 \\ m\neq j}}^{N}(s + k_m)]}$$

* Corresponding author. Tel: (352) 846 2727, fax: (352) 392-4447, e-mail: Hochhaus@UFL.EDU.
† University of Florida.
‡ Current address: Mundipharma GmbH, Mundipharmastrasse2, D-65549Limburg/Lahn.
§ Department of Statistics, College of Liberal Arts, Health Science Center, Gainesville, FL 32610.

10.1021/js980036d CCC: $18.00
Published on Web 07/31/1999

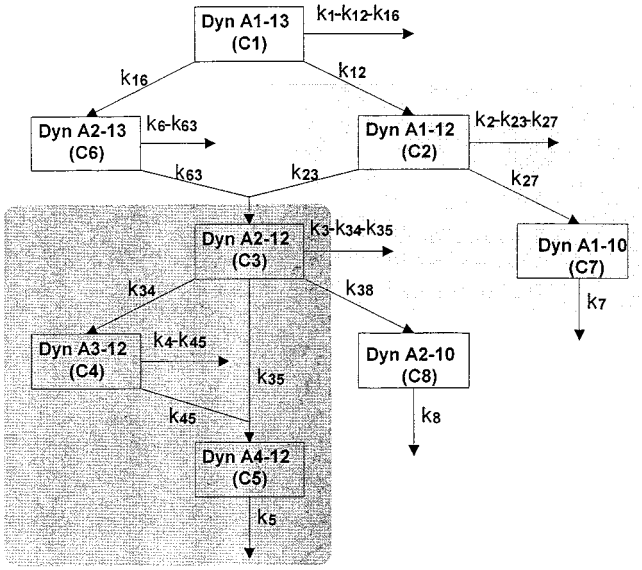

Figure 1—Kinetic model describing the arrangement of metabolite pools in the plasma metabolism of Dyn A 1–13. This model was the basis for compartmental kinetic analysis of Dyn A1–13. Single digit abbreviations (e.g., k_1) are used for degradation rate constants that describe the total outflow of a certain compartment (in this example C1). Rate constants that describe the specific flow from one compartment to another have double digit denominations (e.g., k_{12}) and represent the generation rate constants. The difference between the overall degradation rate constant (e.g., k_1) and relevant generation rate constants (e.g., k_{16} and k_{12}) reflect unknown metabolic events not incorporated into the model. The area in dark gray highlights the metabolic events of Dyn A2–12 under captopril inhibition, the added area in the medium gray shade shows the extension of the model in the metabolic events of Dyn A1–12. The dashed lines signify compartments for which direct data (from HPLC) was not available.

where $d_{s,c}$ is the disposition function for compartment 1 (it is a function of s, the Laplace operator); $\prod$ is the continued product where any term is defined as equal to 1 when the index takes a forbidden value (that is, $i = 1$ in the numerator or $m = j$ in the denominator); $\sum$ is the continued sum where any term is defined as equal to zero when the index takes a forbidden value; k_{1j} is the first-order generation of a metabolite, estimated from relevant generation rate constant; k_i, k_m is the overall degradation rate of a dynorphin fragment, estimated from relevant degradation rate constants; N is the number of the compartments.

The Anti-Laplace of $a_{s,c}$ was obtained by the method of partial fractions.[7] The resulting equations for the final model of Dyn A1−13 (C1) with its metabolites Dyn A1−12 (C2), Dyn A2−12 (C3), Dyn A3−12 (C4), Dyn A2−13 (C6), and Dyn A4−12 (C5) coeluting with Dyn A1−10 (C7) are listed in Appendix 1. The nonlinear curve fitting program Scientist (Micromath, Salt Lake City, Utah) was used to fit the experimental data to the derived equations.

The initial estimates of the degradation rate constants for the parent compound and metabolites (but not generation rate constants) were taken from the estimates obtained from direct incubations of this fragment.[1] Fitting parameters were not allowed to differ from these initial estimates by more than 30% (the maximum variability generally excepted), if not otherwise stated. Initial estimates for the generation rate constant were based on the initial estimates of the degradation rate constants under enzyme inhibition (Table 1). Since some enzyme inhibitors lacked selectivity, these generation rate constants were generally allowed to vary in the curve fitting procedure between 10% and 130% from the initial estimate of the overall rate constant of the relevant metabolic step.

Goodness of fits were evaluated by r^2 and the Model Selection Criterion (MSC), a value based on the Akaike Information Criterion.[8] A local sensitivity analysis was carried out for each of the Dyn derivatives along with some summary measures.[9] The normalized sensitivity coefficient (SC) detailed by Bieniasz and Speiser was calculated for each Dyn derivative (see Appendix 2).[10]

Results and Discussion

Peptides are of importance as therapeutic agents. For a detailed assessment of their therapeutic and clinical properties a detailed knowledge of the metabolic fate of a given peptide is necessary. Approaches employing Michaelis−Menten-type kinetics would depend on the detailed assessment of enzyme kinetics[11] of parent compound and metabolites, as well as the identification and measurement of all relevant (iso-) enzyme concentrations in the investigated biological media. Using Dyn A1−13 as a model compound, we have previously shown that the size of metabolic pools of peptides can be efficiently evaluated over several metabolic generations by noncompartmental analysis (area under the concentration time profiles) and enzyme inhibition studies with parent drug and synthesized metabolites.[1] Within this study, it was also shown that the degradation of Dyn A1−13 and all its metabolites followed apparent first-order kinetics, similar to results for other peptide drugs.[12] It was therefore of interest to test whether a structured compartmental curve fitting approach is helpful for the assessment of complex metabolic events using Dyn A1−13 degradation as an example. Plasma was chosen since it often represents a major metabolic site for peptide drugs given intravenously.[12] In the following, the advantages and disadvantages of such a multicompartmental kinetic analysis are presented in three examples.

Example 1: Identification of the Metabolic Pathways of Peptide Degradation—The following section demonstrates some of the advantages of the multicompartmental modeling approach for the identification of metabolic pathways. As shown in Figure 1, the metabolic fate of Dyn A2−12, one of the main metabolites of Dyn A1−13, produces Dyn A3−12 and Dyn A4−12. To investigate this N-terminal metabolism in more detail, captopril was added to the incubation solution to suppress the C-terminal metabolism of Dyn A2−12 which is dominated by the angiotensin converting enzyme[1] and restricted the metabolic events on the N-terminus. Initial enzyme inhibition studies[1] with the established aminopeptidase inhibitor bestatin were able to fully block the amino-terminal degradation pathway of Dyn A2−12, suggesting a unidirectional degradation from Dyn A2−12 to Dyn A3−12 and subsequently to Dyn A4−12. A comparison of the AUC estimates of Dyn A3−12 obtained from metabolism of Dyn A2−12 under captopril inhibtion with those obtained after direct incubation of Dyn A3−12 contradicted this hypothesis, as the AUC of Dyn A3−12 was smaller than expected for a unidirectional degradation.[1] Quite in agreement, a simulation with the multicompartmental model using rate constants determined from direct degradation of the involved fragments (degradation rate constant under captopril inhibition for Dyn A2−12, Dyn A3−12, Dyn A4−12 using a sequential metabolism from Dyn A2−12 to Dyn A3−12 to Dyn A4−12) failed to describe the data adequately (Figure 2A). Therefore the metabolic pathways differed somewhat from the simple sequential metabolism suggested by bestatin data.

AUC data would support this unidirectional model of metabolic pathways only, if the rate constant of Dyn A3−12 degradation (under captopril: $k_{45} = k_4$) was increased by 10-fold from its initial estimate (obtained from direct degradation of Dyn A3−12). Such an increase in the metabolic rate of Dyn A3−12 could not be fully excluded if the cleavage of Gly2-Gly3 of Dyn A2−12 would facilitate the subsequent cleavage of Gly3-Phe4 of Dyn A3−12 by the same enzyme (the generated Dyn A3−12 would not have to enter the enzymatic pocket for further cleavage). Such cases of "rate enhancement" have been reported in the literature for other peptides.[13] The reference AUC of

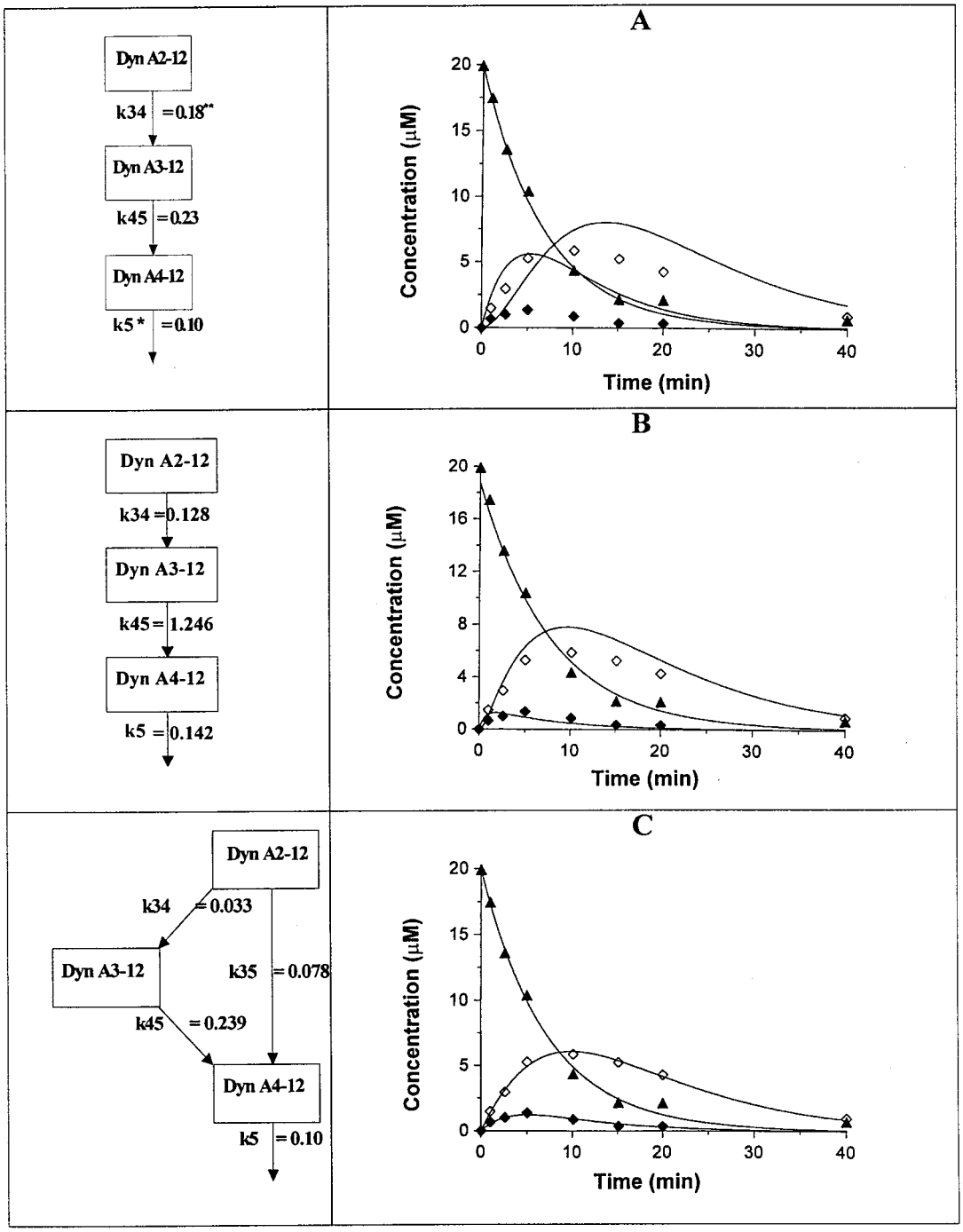

Figure 2—(A) Simulation of concentration–time profiles of Dyn A2–12 (▲) and major metabolites (Dyn A3–12 ◆ and Dyn A4–12 ◇, $r^2 = 0.216$, MSC = –2.781) in human plasma at 37 °C under captopril inhibition using the model of sequential metabolism of Dyn A2–12 into Dyn A3–12 and Dyn A3–12 into Dyn A4–12 with previously obtained rate constants (rate constants under captopril inhibition taken from from Table 1. *k_5 in the presence of captopril was calculated as k_5 (0.17 min^{-1}) minus rate constant associated with captopril sensitive pathway (0.07 min^{-1}): 0.17–0.07 = 0.10 min^{-1} (see Table 1), **k_{34} was based on bestatin enzyme inhibition data ($k_{34} + k_{35}$, see Table 1). (B) Least-squares fit of concentration–time profiles of Dyn A2–12 (▲) and major metabolites (Dyn A3–12 (◆) and Dyn A4–12 (◇), $r^2 = 0.989$, MSC = 3.491) in human plasma at 37 °C under captopril inhibition using model of sequential metabolism of Dyn A2–12 into Dyn A3–12 and increased rate constant k_{45}. k_{34} and k_5 were allowed to float freely (limits for deviation from initial estimates did not apply, see Materials and Methods). (C) Least-squares fit of concentration–time profiles of Dyn A2–12 (▲) and major metabolites (Dyn A3–12 (◆) and Dyn A4–12 (◇), $r^2 = 0.988$, MSC = 5.244) in human plasma at 37 °C under captopril inhibition using the model of simultaneous metabolism of Dyn A2–12 via aminopeptidase and dipeptidylaminopeptidase.

Dyn A3−12 for total conversion from Dyn A2−12 would then be smaller than the AUC observed after direct incubation of Dyn A3−12. For testing this hypothesis with the compartmental model, the rate constant for converting Dyn A3−12 into Dyn A4−12 by the relevant aminopeptidase was assumed to be larger in a series of metabolic events than its estimate obtained from direct degradation of Dyn A3−12. In our data set obtained under captopril inhibition (no C-terminal enzymatic attack), all Dyn A2−12 was then assumed to be converted into Dyn A3−12, and in turn all Dyn A3−12 into Dyn A4−12. However, discrepancies between fitted and observed estimates of Dyn A3−12 or Dyn A4−12 concentration−time profiles were observed in the relevant compartmental model (Figure 2B).

Table 1—Rate Constants of Dynorphin Fragments in Plasma. Listed Is the Overall Rate Constant and the Contribution of Various Enzymatic Systems to the Overall Rate Constant[a]

peptide	*n*	overall rate constant (min^{-1})	rate constant associated with blocked enzyme pathway (min^{-1})			
			GEMSA	bestatin	leucinethiol	captopril
Dyn A1–13	3	0.78 (k_1)	0.61 (k_{12})	0.22 (k_{16})	–	N.T.
Dyn A1–12	3	0.38 (k_2)	N.T.	0.30 (k_{23})	0.28 (k_{23})	0.067 (k_{27})
Dyn A2–13	1	0.99 (k_6)	N.T.	N.T.	N.T.	N.T.
Dyn A2–12	4	0.22 (k_3)	–	0.18 ($k_{34} + k_{35}$)	0.08 (k_{34})	0.07 (k_{38})
Dyn A3–12	2	0.28 (k_4)	N.T.	0.23 (k_{45})	–	0.043
Dyn A4–12	3	0.17 (k_5)	N.T.	0.13	0.09	0.07
Dyn A1–10	1	0.50 (k_7)				

[a] Calculated from ref 1 by transforming half-lives of Table 2 listed in ref 1 into the rate constants associated with the blocked enzyme (associated rate constants of Figure 1 are given in parentheses). NT = not tested; –: no effect.

Table 2—The Formation of Metabolites from Their Parent Compound As Calculated from Multicompartmental Fitting, Enzyme Inhibition Experiments, and Noncompartmental (AUC-based) Analysis[c]

peptide incubated	metabolite formation in % of starting material as calculated by					
	fit	inhibitor	AUC	fit	inhibitor	AUC
Dyn A1–13	79	Dyn A1–12 82	78	10	Dyn A2–13 0 (30[a]	15
Dyn A1–12	78	Dyn A2–12 83 (85)[a]	78	20	Dyn A1–10 19	*b*
Dyn A2–12	15	Dyn A3–12 37 (80)[a]	17	39	Dyn A4–12 28	42

[a] Based on leucinethiol data, bestatin data in brackets. [b] Coeluting with Dyn A4–12. [c] Enzyme inhibition and noncompartmental data taken from ref 1.

These deviations between experimental and modeled concentration−time profile, detected by multicompartmental kinetic analysis, showed the invalidity of the "rate enhanced" unidirectional model.

Finally, a model employing parallel pathways, consequently contradicting the high selectivity of bestatin for aminopeptidase, was investigated using simultaneous least-squares fitting of Dyn A2−12 degradation under ACE inhibition. Rate constants for parallel metabolic pathways were allowed to vary within the limits outlined in the data analysis section. This model adequately described the experimental data (Figure 2C). Thus, the use of the compartmental analysis, suggested the nonspecificity of bestatin, a widely used aminopeptidase inhibitor, very much in agreement with findings by Otero.[14] The consequent use of the more specific inhibitor leucinethiol in the original publication[1] triggered by the results of this fitting procedure supported a smaller involvement of aminopeptidase in the N-terminal metabolism of Dyn A 2−12 (see Table 2). In addition, the analysis suggested a direct degradation of Dyn A2−12 into Dyn A4−12, a pathway which was not revealed by enzyme inhibition studies alone, but in agreement with results of the noncompartmental analysis. These results already argue for one strength of the compartmental approach, namely to incorporate information on the concentration−time relationships in the analysis of complex metabolic events.

Example 2: Detection of Assay Selectivity Problems—Another advantage of simultaneous curve fitting was revealed in the analysis of Dyn A1−12 data. The degradation of Dyn A1−12 under ACE inhibition with captopril using a similar, yet extended, metabolic model described accurately the experimental data (data not shown). Contrary to these results, the concentration−time profile of Dyn A1−12 in naive plasma (no enzyme inhibition) showed a persistent underfit in the profile of Dyn A4−12 in both visual assessment and the correlation statistics on the data set of Dyn A4−12 (Figure 3A).

The hypothesis was that the poor fit might be attributed to the small amounts of generated Dyn A1−10 which was present in the Dyn A1−12 but not in the Dyn A2−12 incubations. Dyn A1−10 and Dyn A4−12 were known to have very similar chromatographic retention profiles in the applied chromatographic system[1] and therefore probably coelute. To investigate the possibility of this peak impurity causing the observed underfit, the concentration−time profile of Dyn A4−12, Dyn A1−10, and their cumulative profile were simulated using the rate constant estimates of k_{27}, k_7, k_2, k_{35}, k_{45}, k_5 from Table 1 (for explanation of abbreviations, see Figure 1) obtained by separate degradation of the relevant dynorphin fragments with or without enzyme inhibitors. The cumulative profile closely resembled the observed data points (Figures 3B and 3C). A fit of Dyn A1−12 degradation in naive plasma taking the impurity into account resulted in a good description of the observed data points (Figure 3C). Although the contributions of Dyn A1−10 to the overall AUC was minor (see relevant degradation rate constants), it illustrates the dependency of noncompartmental kinetic data on chromatographic resolution. Unfortunately, the likelihood of chromatographic impurity increases with the number analytes to be separated; as this was the case for the degradation of Dyn A1−13 for which a total of 17 metabolites were identified. Since all metabolic processes followed apparent first-order kinetics, the multicompartmental modeling approach was instrumental in detecting coelution of chromatographic peaks which none of the other methods would have been able to detect.

Example 3: Application of the Model to Data Sets Describing Entire Degradation Pathways—The above sections showed several advantages of the simultaneous curve fitting procedures in evaluating isolated events in the analysis of complex metabolic systems. In the following the ability to describe and analyze entire degradation pathways is assessed. The applied method, presented so far, incorporated degradation constants based on enzyme inhibition studies into the compartmental analysis to ensure valid initial estimates for the rate constants during the curve fitting procedure. This ensured that the fitting procedure stayed within limits imposed by direct degradation or valid enzyme inhibition experiments of parent drug and metabolites. The same procedure applied to the entire degradation pathway resulted in fits shown in Figure 4 and rate constants observed under rigid limits in Table 3. The agreement between experimentally found and predicted values (Figure 4) strongly supports the validity of the identified metabolic pathway (Figure 1). Table 2 compares the results of the multicompartmental approach, noncompartmental method, and results of the enzyme inhibition studies. Here, the rate constants of degradation or generation obtained from above fitting procedures of Dyn A2−

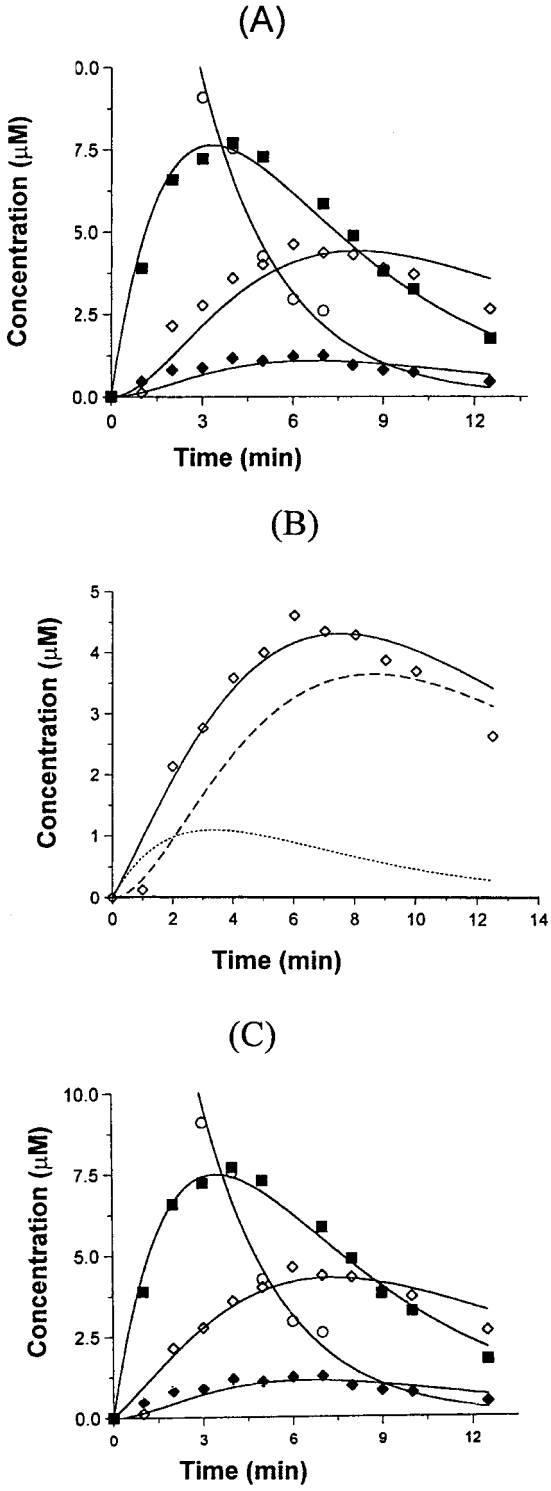

Figure 3—(A) Least-squares fit of concentration–time profiles of Dyn A1–12 (○) and major metabolites (Dyn A2–12 ■, Dyn A3–12 ◆, and assumed Dyn A4–12 (see Figure 3B for more information on "mixed peak") ◇, $r^2 = 0.996$, MSC = 4.81) in human plasma at 37 °C based on the model of Figure 1. (B) Simulation of concentration–time profiles of Dyn A4–12 (- - -) and Dyn A1–10 (•••) after incubation of Dyn A1–12 with overlay of mixed peak (◇). Concentration–time profiles were simulated using unfitted initial estimates of the relevant rate constants (Table 1) or estimates obtained in Figure 2C: $k_7 = 0.5$ min^{-1}, $k_{27} = 0.067$ min^{-1}, $k_{23} = 0.30$ min^{-1}, $k_{34} = 0.008$ min^{-1}, $k_4 = 0.28$ min^{-1}, $k_{45} = 0.239$ min^{-1}, $k_{35} = 0.078$ ($r^2 = 0.987$, MSC = 0.861). (C) Least-squares fit of concentration–time profiles of Dyn A1–12 (○) and major metabolites (Dyn A2–12 ■, Dyn A3–12 ◆, and mixed Dyn A4–12 and Dyn A1–10 ◇, $r^2 = 0.998$, MSC = 5.213) in human plasma at 37 °C based on the model of Figure 1, accounting for coelution of Dyn A4–12 and Dyn A1–10.

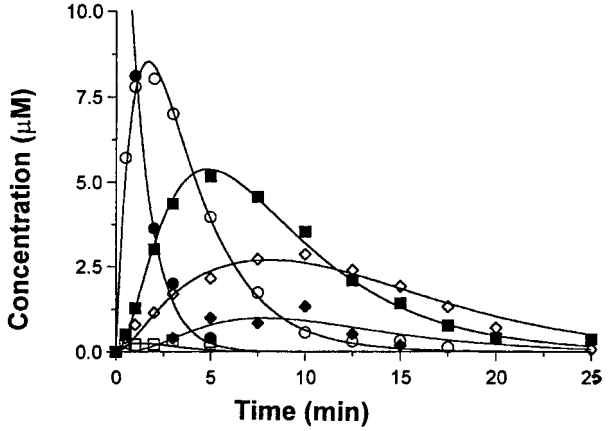

Figure 4—Least-squares fit of concentration–time profiles of Dyn A1–13 (●) and major metabolites (Dyn A1–12 ○, Dyn A2–13 □, Dyn A2–12 ■, Dyn A3–12 ■, and coeluting Dyn A4–12 and Dyn A1–10 ◇, $r^2 = 0.995$, MSC = 4.485) in human plasma at 37 oC accounting for coelution of Dyn A4–12 and Dyn A1–10.

Table 3—Initial Concentration and Rate Constants (min^{-1}) of Dyn A1–13 and Metabolic Fragments in Plasma Fitted to the Model Depicted in Figure 1[a]

parameter	rigid limits*	free-floating parameters**
degradation of A1–13 (k_1)	0.901 ± 0.013	0.892
generation of A2–13 (k_{16})	0.091 ± 0.043	0.015
generation of A1–12 (k_{12})	0.713 ± 0.082	0.702
degradation of A1–12 (k_2)	0.299 ± 0.002	0.384
generation of A2–12 (k_{63})	0.792 ± 0.001	80.9
generation of A1–10 (k_{27})	0.059 ± 0.001	2.2×10^{217}
degradation of A1–10 (k_7)	0.502 ± 0.004	2.1×10^{53}
degradation of A2–13 (k_6)	1.007 ± 0.014	0.178
generation of A2–12 (k_{23})	0.232 ± 0.001	0.266
degradation of A2–12 (k_3)	0.220 ± 0.004	0.197
generation of A3–12 (k_{34})	0.032 ± 0.001	0.119
generation of A4–12 (k_{35})	0.077 ± 0.001	0.227
degradation of A3–12 (k_4)	0.278 ± 0.003	0.536
generation of A4–12 (k_{45})	0.210 ± 0.002	2.53×10^{-16}
degradation of A4–12 (k_5)	0.170 ± 0.004	0.313

[a] Parameters were kept in rigid limits as outlined in the data analysis section or allowed to vary freely ("float") between zero and infinity. *$n = 6$, **$n = 1$.

12, Dyn A1−12, and Dyn A1−13 (Table 3) were used to calculate the % of Dyn A 1−13, Dyn A 1−12, or Dyn A2−12 entering a specific metabolite pool. A good agreement between the compartmental curve fitting approach and the other two methods[1] suggests that one strength of the structured multicompartmental approach is the ability to test the correctness of metabolic pathways suggested by other methods.

Removing the limits of the curve fitting procedure, while retaining the initial estimates for the rate constants, probed how well the compartmental model could stand on its own. After least-squares optimization, the majority of rate constants compared to the rate constants obtained with imposed limits (Table 3). However, minor metabolites, rate constants of metabolites for which no direct data were available and/or fast degradation processes (Dyn A2−13 and Dyn A1−10, Table 3) deviated markedly. This suggests that the unrestricted use of parameter estimates carries the danger of "overfitting" the data (e.g., of minor metabolites) to suit a certain model and the loss of identifiability. Although the resulting fit is good, the predicted rate constants are irrelevant, since they do not possess any practical significance (Table 3) when compared with rate constants obtained from enzyme inhibition studies. Another attempt was made to perform the fitting procedure without

Table 4—Results of Local Sensitivity Analysis

	k_{12}	k_{16}	k_{23}	k_{27}	k_{34}	k_{35}	k_{45}	k_5	k_{63}	k_7
Cl	11.0	1.40	0.00	0.00	0.00	0.00	0.00	0.00	0.00	0.00
C2	0.26	0.12	3.27	0.83	0.00	0.00	0.00	0.00	0.00	0.00
C3	2.82	0.78	0.82	0.28	0.34	0.81	0.00	0.00	3.95	0.00
C4	0.22	0.11	0.59	0.21	0.79	0.51	0.90	0.00	0.07	0.00
C6	7.79	0.87	0.00	0.00	0.00	0.00	0.00	0.00	3.57	0.00
C5 C7	1.21	0.33	2.88	0.76	0.18	0.62	0.00	1.32	0.44	1.43
overall	3.88	0.60	1.89	0.52	0.44	0.65	0.90	1.32	2.65	1.43

good initial estimates for the rate constants (setting all to 0.5 or 1) and without limits. Under these circumstances the data for Dyn A1−13 and its metabolites could not be fitted to the model outlined in Figure 1 (data not shown). More detailed evaluation of the fits described in Figure 4 by local sensitivity analysis identified k_{12} (linked to k_1), k_{63}, and k_{23} as the most sensitive rate constants, while k_{16}, k_{27}, k_{34}, k_{35} represent overall the least sensitive (see Appendix 2 for a more detailed description of the method and Table 4 for a representation of the results of the analysis). Thus, the sensitivity analysis confirmed the presence of general identifiability problems, similar to those indicated by comparing results of rigid and free-floating parameter estimations. The sensitivity analysis reemphasized that the isolated use of such complex models is not feasible. However, the use of experimentally derived estimates of rate constants (e.g., obtained from incubations of synthesized metabolites in the presence or absence of enzyme inhibitors, see Materials and Methods for more detail) in the model is very helpful in probing for the acceptability of a metabolic scheme proposed by the other methods. Thus, structured multicompartmental modeling approaches will be useful in the evaluation of complex peptide degradation pathways when used hand in hand with alternative forms of analysis, such as enzyme inhibition studies and noncompartmental analytical approaches.

In conclusion, the presented apparent first-order multicompartmental approach has several advantages. It is relatively rapid and focuses only on the metabolically relevant processes. The presented model can be extended to include Michaelis−Menten kinetics when necessary. However, such an extension would add several parameters which have to based on further experiments and should only be applied when necessary (i.e., the half-life changes in the experimental concentration range). The application of the compartmental approach in the evaluation of the metabolic fate of Dyn A1−13 and related fragments helped to identify a lack of chromatographic resolution and a low selectivity of one of the enzyme inhibitors employed in the study. It further was able to support the correctness of the proposed metabolic pathways.

Peptide metabolism has been generally evaluated by biochemists with the help of enzyme inhibition studies. The application of pharmacokinetic tools such as noncompartmental approaches have been recently incorporated into such investigations.[1] The results presented in this study suggest distinct advantages of the compartmental analysis for evaluating complex metabolic events. Because of the inherent possible pitfalls of all three methods, the combined use of all approaches might be best suited to assess complex metabolic degradation patterns of peptides in a detailed fashion.

Appendix 1

Equations Employed for the Simultaneous Fitting of Dyn A1−13 and Its Main Metabolites According to Figure 1—*For Dyn A1−13:* $C1 = C0\ \exp((-k_1)t)$

For Dyn A1−12: $C2 = k_{12}C0/(k_1 - k_2)(\exp((-k_2)t) - \exp((-k_1)t))$

For Dyn A2−13: $C6 = k_{16}C0/(k_1 - k_6)(\exp((-k_6)t) - \exp((-k_1)t))$

For Dyn A2−12: $C3 = k_{12}k_{23}C0/((k_2 - k_3)(k_1 - k_3))\exp((-k_3)t) + k_{12}k_{23}C0/((k_3 - k_2)(k_1 - k_2))\exp((-k_2)t) + k_{12}k_{23}C0/((k_3 - k_1)(k_2 - k_1))\exp((-k_1)t) + k_{16}k_{63}C0/((k_6 - k_3)(k_1 - k_3))\exp((-k_3)t) + k_{16}k_{63}C0/((k_3 - k_6)(k_1 - k_6))\exp((-k_6)t) + k_{16}k_{63}C0/((k_3 - k_1)(k_6 - k_1))\exp((-k_1)t)$

For Dyn A3−12: $C4 = k_{12}k_{23}k_{34}C0/((k_3 - k_4)(k_2 - k_4)(k_1 - k_4))\exp((-k_4)t) + k_{12}k_{23}k_{34}C0/((k_4 - k_3)(k_2 - k_3)(k_1 - k_3))\exp((-k_3)t) + k_{12}k_{23}k_{34}C0/((k_4 - k_2)(k_3 - k_2)(k_1 - k_2))\exp((-k_2)t) + k_{12}k_{23}k_{34}C0/((k_4 - k_1)(k_3 - k_1)(k_2 - k_1))\exp((-k_1)t) + k_{16}k_{63}k_{34}C0/((k_3 - k_4)(k_6 - k_4)(k_1 - k_4))\exp((-k_4)t) + k_{16}k_{63}k_{34}C0/((k_4 - k_3)(k_6 - k_3)(k_1 - k_3))\exp((-k_3)t) + k_{16}k_{63}k_{34}C0/((k_4 - k_6)(k_3 - k_6)(k_1 - k_6))\exp((-k_6)t) + k_{16}k_{63}k_{34}C0/((k_4 - k_1)(k_3 - k_1)(k_6 - k_1))\exp((-k_1)t)$

For Coeluting Dyn A4−12 (C5) and Dyn A1−10 (C7): $C5 = k_{12}k_{23}k_{35}C0/((k_3 - k_5)(k_2 - k_5)(k_1 - k_5))\exp((-k_5)t) + k_{12}k_{23}k_{35}C0/((k_5 - k_3)(k_2 - k_3)(k_1 - k_3))\exp((-k_3)t) + k_{12}k_{23}k_{35}C0/((k_5 - k_2)(k_3 - k_2)(k_1 - k_2))\exp((-k_2)t) + k_{12}k_{23}k_{35}C0/((k_5 - k_1)(k_3 - k_1)(k_2 - k_1))\exp((-k_1)t) + k_{16}k_{63}k_{35}C0/((k_3 - k_5)(k_6 - k_5)(k_1 - k_5))\exp((-k_5)t) + k_{16}k_{63}k_{35}C0/((k_5 - k_3)(k_6 - k_3)(k_1 - k_3))\exp((-k_3)t) + k_{16}k_{63}k_{35}C0/((k_5 - k_6)(k_3 - k_6)(k_1 - k_6))\exp((-k_6)t) + k_{16}k_{63}k_{35}C0/((k_5 - k_1)(k_3 - k_1)(k_6 - k_1))\exp((-k_1)t) + k_{12}k_{23}k_{34}k_{45}C0/((k_4 - k_5)(k_3 - k_5)(k_2 - k_5)(k_1 - k_5))\exp((-k_5)t) + k_{12}k_{23}k_{34}k_{45}C0/((k_5 - k_4)(k_3 - k_4)(k_2 - k_4)(k_1 - k_4))\exp((-k_4)t) + k_{12}k_{23}k_{34}k_{45}C0/((k_5 - k_3)(k_4 - k_3)(k_2 - k_3)(k_1 - k_3))\exp((-k_3)t) + k_{12}k_{23}k_{34}k_{45}C0/((k_5 - k_2)(k_4 - k_2)(k_3 - k_2)(k_1 - k_2))\exp((-k_2)t) + k_{12}k_{23}k_{34}k_{45}C0/((k_5 - k_1)(k_4 - k_1)(k_3 - k_1)(k_2 - k_1))\exp((-k_1)t) + k_{16}k_{63}k_{34}k_{45}C0/((k_4 - k_5)(k_3 - k_5)(k_6 - k_5)(k_1 - k_5))\exp((-k_5)t) + k_{16}k_{63}k_{34}k_{45}C0/((k_5 - k_4)(k_3 - k_4)(k_6 - k_4)(k_1 - k_4))\exp((-k_4)t) + k_{16}k_{63}k_{34}k_{45}C0/((k_5 - k_3)(k_4 - k_3)(k_6 - k_3)(k_1 - k_3))\exp((-k_3)t) + k_{16}k_{63}k_{34}k_{45}C0/((k_5 - k_6)(k_4 - k_6)(k_3 - k_6)(k_1 - k_6))\exp((-k_6)t) + k_{16}k_{63}k_{34}k_{45}C0/((k_5 - k_1)(k_4 - k_1)(k_3 - k_1)(k_6 - k_1))\exp((-k_1)t)$

$C7 = k_{12}k_{27}C0/((k_2 - k_7)(k_1 - k_7))\exp((-k_7)t) + k_{12}k_{27}C0/((k_7 - k_2)(k_1 - k_2))\exp((-k_2)t) + k_{12}k_{27}C0/((k_7 - k_1)(k_2 - k_1))\exp((-k_1)t)$

Appendix 2

Calculation of Sensitivity Coefficients—A local sensitivity analysis was carried out for each Dyn along with some summary measures, e.g., see Rabitz for a detailed description.[9] The normalized sensitivity coefficient (SC) detailed in Bieniasz and Speiser was calculated for each Dyn i as[10]

$$SC_{ij}(t) = \frac{\partial \ln C_i(t)}{\partial \ln k_j}\Big|_{k_j = k'_j} \qquad (1.1)$$

where i, $i = 1, 2, 7$, the rate constant j corresponds to the set $j = \{12, 16, 23, 27, 34, 35, 45, 5, 63, 7\}$, and the equations for the C_i's are given in Appendix 1. The values for the k_j are given in Table 3. Furthermore, the SC for C5 and C7 was calculated jointly, since C5 and C7 were considered additive, i.e., the joint SC was given by $SC_{5,j} + SC_{7,j}$. The rate constants k_1, k_2, k_3, k_4, k_6 were linked to the other rate constants through the equations $k_1 = k_{16} + k_{12} + k_{1u}$ or $k_2 = k_{23} + k_{27} + k_{2u}$ or $k_3 = k_{34} + k_{35} + k_{3u}$ or $k_4 = k_{45} + k_{4u}$ or $k_6 = k_{63} + k_{6u}$, where k_{1u}, k_{2u}, k_{3u}, k_{4u}, k_{6u} represents degradation of specific metabolites not included in known metabolic pathways. The absolute magnitude of the SC's were summarized across time as

$$\mathrm{ASC}_{i,j} = \sum_{k=1}^{7} |\mathrm{SC}_{i,j}(t_k)|, \qquad (1.2)$$

where $t_1 = 1$, $t_2 = 2$, $t_3 = 5$, $t_4 = 10$, $t_5 = 20$, $t_6 = 30$, and $t_7 = 40$. The results are given in the body of Table 4. The values were then averaged for each rate constant in order to provide a global measure of sensitivity across time. To calculate the overall mean sensitivity, we did not average in the values of $\mathrm{ASC}_{i,j} = 0$.

References and Notes

1. Mueller, S.; Hochhaus, G. Metabolism of dynorphin A1−13 in human blood and plasma. *Pharm. Res.* **1995**, *12*, 1165−1170.
2. Chavkin, C.; Goldstein, A. Specific receptor for the opioid peptide dynorphin: Structure−activity relationship. *Proc. Natl. Acad. Sci. U.S.A.* **1981**, *78*, 6543−6547.
3. Takemori, A. E.; Loh, H. H.; Lee, N. N. Suppression by dynorphin A and [des-Tyr1]dynorphin A peptides of the expression of opiate withdrawal and tolerance in morphine-dependent mice. *J. Pharm. Exp. Ther.* **1993**, *266*, 121−124.
4. Mueller, S.; Chang-Sing-Pang, F. B.; Hochhaus, G. Displacement of [^{3}H]-L-glutamate in Rat Brain Membranes by Metabolic Dynorphin Fragments. *Die Pharmazie* **1998**,
5. Quillan, J. M.; Sadee, W. Dynorphin Peptides; Antagonists of melanocortin receptors. *Pharm. Res.* **1997**, *14*, 713−719.
6. Henriksen, J. H. Kinetics of whole-body and organ degradation. In *Degradation of bioactive substances: Physiology and Pathophysiology*; Henriksen, J. H., Ed.; CRC: Boca Raton, 1991; pp 3−32.
7. Gibaldi, M.; Perrier, D. *Pharmacokinetics*; 2nd ed.; Raven: New York, 1982.
8. *Micromath, Scientist, Mathematical modeling/differential and nonlinear equations*; MicroMath Scientific Software: Salt Lake City, UT, 1993; pp 193−194.
9. Rabitz, H. Systems analysis at the molecular scale. *Science* **1989**, *246*, 221−246.
10. Bieniasz, L. K.; Speiser, B. Use of sensitivity analysis methods in the modelling of electrochemical transients. Part 1. Gaining more insight into the behaviour of kinetic models. *J. Electroanal. Chem.* **1998**, *441*, 221−246.
11. Bausback, H. H.; Ward, P. E. Degradation of low molecular-weight opioid peptides by vascular plasma membrane aminopeptidase M. *Biochim. Biophys. Acta* **1986**, *882*, 437−444.
12. Powell, M. F. Peptide stability in drug development: A comparison of peptide reactivity in different biological media. *J. Pharm. Sci.* **1992**, *81*, 731−735.
13. Walker, R.; Krishnaswamy, S. The activation of prothrombin by the prothrombinase complex. The contribution of the substrate-membrane interaction to catalysis. *J. Biol. Chem.* **1994**, *274*, 41−50.
14. Otero, M. J.; Iglesias, T.; Fuentes, J. A. Hypoalgesic action of bestatin analogues that inhibit central aminopeptidases, but not neutral endopeptidases. *Neuropeptides* **1993**, *25*, 175−182.

Acknowledgments

This study was supported in part by Neurobiological Technologies Incorporated, Richmond, CA. The work of A.H. was supported in part by NIH General Clinical Research Center Grant RR0082.

JS980036D